UNIFIED GNSS-R FORMULATION INCLUDING COHERENT AND INCOHERENT SCATTERING COMPONENTS

H. Carreno-Luengo, A. Camps
Universitat Politècnica de Catalunya – BarcelonaTech Remote Sensing Lab. and IEEC/CTE-UPC, UPC
E-mail: hugo.carreno@tsc.upc.edu, camps@tsc.upc.edu

ABSTRACT

Global Navigation Satellite Systems Reflectometry (GNSS-R) is a sort of multi-static radar using navigation signals as signals of opportunity. Due to the large number of transmitting satellites multiple scattering points over the Earth's surface can be simultaneously tracked, which provides wide-swath and improved spatio-temporal sampling over current space-borne radar altimetry missions. The lack of experimental datasets from space covering signals from multiple constellations (GPS, GLONASS, Galileo and Beidou) at dual-band (L1 and L2), and dual-polarization (Right and Left Hand Circular Polarization: RHCP and LHCP), over the ocean, land, and cryosphere remains a bottleneck to further develop these techniques. ^{3}Cat-2 is a 6 unit (3 x 2 elementary blocks of 10 x 10 x 10 cm^3) cubesat mission designed and implemented at the Universitat Politècnica de Catalunya-BarcelonaTech. It will be launched in late July 2016. During one of the two stratospheric balloon flights of the ^{3}Cat-2 payload, the P(Y) and C/A ReflectOmeter (PYCARO), it was found that the received signal power was nearly constant with the balloon height. This revealed the presence of a strong coherent component. This work presents the derivation of a unified equation to account for both incoherent and coherent scattering contributions.

Index Terms— GNSS-R, cubesat, stratospheric balloon, BEXUS, coherent scattering

1. INTRODUCTION

The first space-borne measurement of an Earth-reflected GPS signal took place in an opportunistic manner during the Space-borne Imaging Radar-C (SIR-C) mission in 1994 [1]. The collected data helped to estimate the Signal-to-Noise Ratio (SNR) during the preparatory activities of the SAC-C and CHAMP missions. CHAMP collected reflected GPS signals during the GPS radio-occultations operational mode at very low elevation angles. The first space-borne proof-of-concept of GNSS Reflectometry from space took place with the L1 C/A code GPS data logger on-board the UK-DMC [2]. Samples of GPS signals reflected over ocean, land and ice were collected, downloaded and processed on-ground. The nadir-looking antenna was composed of three LHCP GPS patches at L1 (1575.42 MHz), with a total gain at boresight of ~12 dB. In June 2014 the UK TechDemoSat-1 (TDS-1) from SSTL was launched, a multi-payload microsatellite (770 x 500 x 900 mm^3) including the SGR-ReSI GNSS-R instrument. At present, at least three other space-borne missions are approved or under-study: NASA's Cyclone Global Navigation Satellite System (CyGNSS), ESA's GNSS rEflectometry Radio Occultation and Scatterometry experiment on-board International Space Station (GEROS-ISS), and the ^{3}Cat-2 cubesat mission (Fig. 1) from the Universitat Politècnica de Catalunya [3].

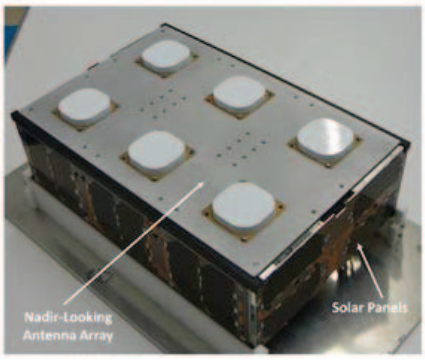

Fig. 1. Picture of ^{3}Cat-2 flight model showing the nadir-looking antenna array integrated in one of the sides of the structure.

Section 2 presents a brief summary of the experimental results that triggered this work. Section 3 presents an extension of the classical GNSS-R equation [4] to include coherent GNSS-R scattering. Section 4 applies these results to different scenarios, and Section 5 summarizes the main conclusions of this work.

2. EXPERIMENTAL EVIDENCES

Figure 2 shows two of the surprising results of the BEXUS 17 field experiment:

- on one side the temporal samples of the received power (peak of the cross-correlation or waveform) jump around four different values, which can only be attributed to different scattering mechanisms in the soil and canopy, and

- on the other side, the received power for each mechanism does not decrease with the balloon height, as it would be expected ($1/R_2^2$), which suggests that the received power has a non-negligible coherent component.

A third surprising evidence came from BEXUS 19, when a coherent component was also found for the co-polar scattered signal. Figure 3 shows the polarimetric ratios defined as $\langle|Y_{RL}^{ref}|^2\rangle / \langle|Y_{RR}^{ref}|^2\rangle$ during the floating phase (height = 27 km) for GLONASS L1 C/A, L2 C/A, and L2 P, and Galileo E1 BC. Similar results were found for GPS signals.

Following the bistatic radar equation, the received power (waveform, in units of power) can be expressed as [4]:

$$\langle|Y_{RL}^{ref}|^2\rangle = \frac{P_T\lambda^2}{(4\pi)^3}\iint \frac{D_T(\vec{\rho})D_R(\vec{\rho})|\chi(\tau-(R_0+R)/c, f_D(\vec{\rho})-f_c)|^2\sigma^0(\vec{\rho})}{R_T^2(\vec{\rho})R_R^2(\vec{\rho})}d^2\rho, \quad (1)$$

where P_T is the transmitted power, D_T and D_R are the transmitter and receiver antenna directivities at the point $\vec{\rho}$ over the surface, R_T and R_R are the distance from the transmitter and the receiver to point $\vec{\rho}$, $|\chi(\tau,f)|^2$ is the Woodward ambiguity function, and σ^0 is the radar cross-section density. In Eqn. (1) the integral extends over an infinite surface, but in practice the scattering is originated over an area around the nominal specular reflection point. Incoherent scattering comes from a large number of individual scatterers within an elliptical area called the glistening zone, similarly to the Sun scattering over the roughed sea surface comes from an ellipse [5].

The size of this ellipse increase with the surface roughness. On the other hand, the coherent scattering area is usually defined as the rule of thumb as the first Fresnel zone. This point will be revised later.

The separation between coherent and incoherent scattering is usually found in the literature as two separate equations, apparently not connected: Eqn. (1) is used for the incoherent component (now Eqn. (2a) below), and Eqn. (2b) is used for the coherent component:

$$\langle|Y_{RL}^{ref,incoh}|^2\rangle = \frac{P_T\lambda^2}{(4\pi)^3}\iint \frac{D_T(\vec{\rho})D_R(\vec{\rho})|\chi(\tau-(R_0+R)/c, f_D(\vec{\rho})-f_c)|^2\sigma^0(\vec{\rho})}{R_T^2(\vec{\rho})R_R^2(\vec{\rho})}d^2\rho, \quad (2a)$$

$$\langle|Y_{RL}^{ref,coh}|^2\rangle = \frac{P_T\lambda^2}{(4\pi)^2}\frac{D_T(\vec{\rho}_{sp})D_R(\vec{\rho}_{sp})\Gamma(\vec{\rho}_{sp})}{\left(R_T(\vec{\rho}_{sp})+R_R(\vec{\rho}_{sp})\right)^2}, \quad (2b)$$

where Γ is the reflection coefficient at the specular reflection point $\vec{\rho}_{sp}$, and it is given by:

$$\Gamma = |\Re|^2 e^{-2k^2\sigma^2\cos^2\theta}, \quad (3)$$

Strictly speaking, in Eqn. (3), a perfect specular reflection implies $\sigma = 0$, but there is experimental evidence that Eqns. (2b) and (3) hold for small surface roughness, even at large incidence angles.

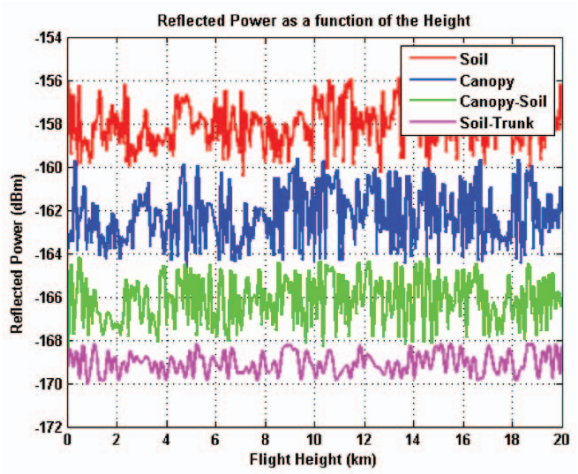

Fig. 2. Reflected power evolution as a function of the time, expressed as flight height during the ascend path, and the scattering media: soil, canopy, canopy-soil, and soil-trunk [6].

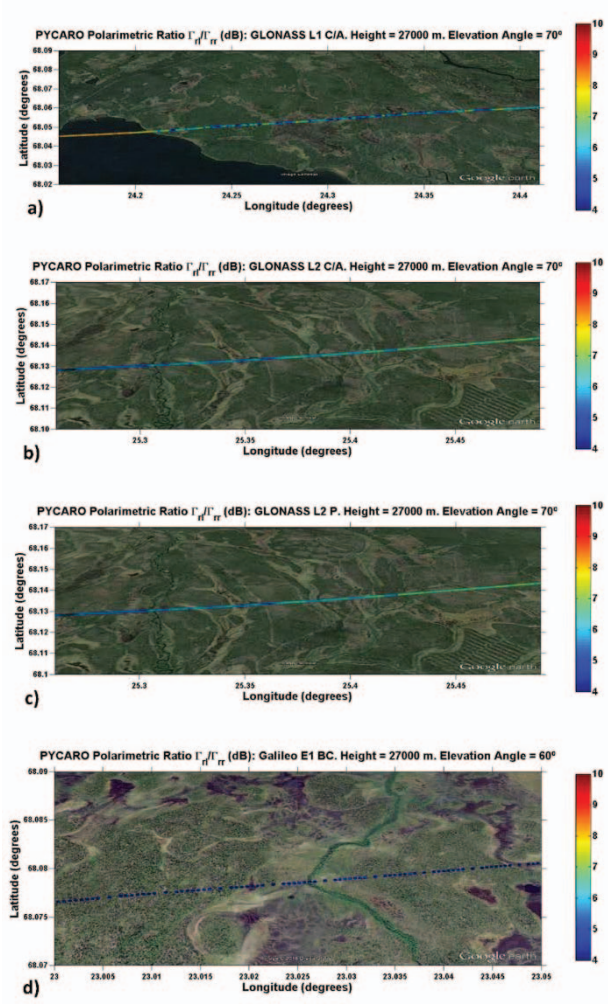

Fig. 3. Measured polarimetric ratios for a flight height of 27,000 m for (a) GLONASS L1 C/A, (b) GLONASS L2 C/A, (c) GLONASS L2 P and (d) Galileo E1 BC [8].

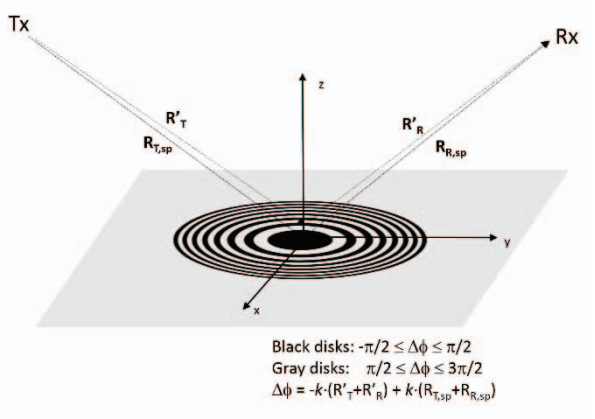

Fig. 4. Scattering geometry and contributions to the coherent scattering from different Fresnel zones.

where $\Re$ is the Fresnel reflection coefficient, $k = 2\pi/\lambda$ is the wavenumber, σ is the rms surface roughness, and θ is the incidence angle. In the following section the connection between Eqns. (2a) and (2b) is made in a rigorous, but intuitive way.

3. UNIFIED SCATTERING FRAMEWORK

In general, the scattered electromagnetic field contains both a coherent and an incoherent component in different proportions. The bistatic scattering coefficient σ_{RL}^0 consists of a coherent component $\sigma_{RL}^{0,coh}$ and an incoherent component $\sigma_{RL}^{0,incoh}$ [9, pp. 200], where superscripts *coh* and *incoh* indicate the coherent and incoherent components, respectively, and subscripts *R* and *L* represent the incident polarization (Right Hand Circular Polarization), and the scattered polarization (Left Hand Circular Polarization), respectively. Therefore, the reflected power waveforms or the Delay Doppler Maps are composed by the sum of an incoherent and a coherent contribution, which can be naturally obtained by replacing σ^0 in Eqn. (1) by $\sigma_{RL}^0 = \sigma_{RL}^{0,incoh} + \sigma_{RL}^{0,coh}$. Then, the integral can be split in two terms, the first one being Eqn. (2a), and the second one:

$$\langle |Y_{RL}^{ref,coh}|^2 \rangle = \frac{P_T \lambda^2}{(4\pi)^3} \iint \frac{D_T(\vec{\rho}) D_R(\vec{\rho}) |\chi(\tau-(R_0+R)/c, f_D(\vec{\rho})-f_c)|^2 \sigma_{RL}^{0,coh}(\vec{\rho})}{R_T^2(\vec{\rho}) R_R^2(\vec{\rho})} d^2\rho. \quad (4)$$

The coherent component appears when the surface roughness is small enough so that the phase of the scatterers around the specular reflection point (origin of coordinates in Fig. 4) is preserved. In this case, each scatterer contributes to the electric field at the receiver with a phase difference as compared to the specular reflection point, which is given by $\Delta\phi = -k \cdot \{(R'_T + R'_R) - (R_{T,sp} + R_{R,sp})\}$. As the point in the surface moves away from the origin, the phase difference increases (in absolute value) and the contribution decreases in amplitude, but starts subtracting to the received electric field. In the so-called first Fresnel zone the scattered signals arrive at the receiver with a phase shift up to 90° (inner black disk). In the second Fresnel zone (smaller gray annulus) signals subtract to the total field, since they arrive with a phase shift between 90° and 270°. In the third Fresnel zone (smallest black annulus) signals add, since they arrive with a phase shift between 270° and 450°, and so on.

Since as the contributions of the scatterers decrease quickly as they get farther away from the specular reflection point, despite Eqn. (4) must be integrated over the whole XY plane, Since the dimensions of the first Fresnel zones are much smaller than the distances to the transmitter and receiver, it can be assumed that the antenna directivities, $\sigma_{RL}^{0,coh}$, R_T and R_R are nearly constant, $|\chi(\tau - (R_0 + R)/c\,, f_D(\vec{\rho}) - f_c)|^2 \approx 1$, and Eqn. (4) can be evaluated as:

$$\langle |Y_{RL}^{ref,coh}|^2 \rangle = \frac{P_T \lambda^2}{(4\pi)^3} \frac{D_T(\vec{\rho}_{sp}) D_R(\vec{\rho}_{sp}) \sigma_{RL}^{0,coh}(\vec{\rho}_{sp})}{R_T^2(\vec{\rho}_{sp}) R_R^2(\vec{\rho}_{sp})} \iint d^2\rho. \quad (5)$$

Equation (5) extends over the whole XY plane. It is worth to consider that $\iint d^2\rho$ is the area obtained by integrating $d^2\rho$ in elliptical disks o increasing size with semi-axes $\alpha\, H_0$ and $\alpha\, H_0/\cos\theta_i$, being H_0 the first Fresnel zone defined as:

$$H_0 = \sqrt{\lambda \frac{R_{T,sp} R_{R,sp}}{R_{T,sp} + R_{R,sp}}}. \quad (6)$$

That is, for a flat surface, when $\alpha \to \infty$, Eqn. (5) tends Eqn. (2b). It is also interesting to find the value of α for which Eqn. (5) is also equal to Eqn. (2b). This value of α will determine the equivalent region from where the coherent scattering component is coming from.

In the reflection direction, the bistatic radar cross-section σ_{RL}^{coh} of a perfectly conducting elliptical disk of area A is given in [10], but in the specular reflection direction it can be demonstrated that it is simply:

$$\sigma = \frac{4\pi}{\lambda^2} A'^2. \quad (7)$$

where A' is the projected area of the elliptical disk (a=$\alpha\, H_0$ and b=$\alpha\, H_0/\cos\theta_i$) in the receiver's direction. Actually, it is straightforward to show that A' is equal to the area of a circle with radius $\alpha\, H_0$. Therefore, replacing $A' = \pi(\alpha\, H_0)^2$ in Eqn. (7) the radar cross-section becomes:

$$\sigma = \frac{4\pi}{\lambda^2} \cdot [\pi(\alpha\, H_0)^2]^2, \quad (8)$$

In the case of a non-conducting surface, the reflectivity radar-cross section (Eqn. (8)) must be decreased by the reflection coefficient given in Eqn. (3), and then Eqn. (5) becomes identical to Eqn. (2b).

$$\langle |Y_{RL}^{ref,coh}|^2 \rangle = \frac{P_T \lambda^2}{(4\pi)^2} \frac{D_T(\vec{\rho}_{sp}) D_R(\vec{\rho}_{sp}) \Gamma(\vec{\rho}_{sp})}{\left(R_T(\vec{\rho}_{sp}) + R_R(\vec{\rho}_{sp})\right)^2} \cdot \pi^2 \cdot \alpha^4 \cdot, \quad (9)$$

if $\alpha = 1/\sqrt{\pi}$ in Eqn. (9). This means that, the equivalent area from which the coherent scattered signal comes from is $1/\sqrt{\pi}$ times the projection over the surface of the First Fresnel zone, an ellipse of axes $2a = \frac{2}{\sqrt{\pi}} H_0$ and $2b = \frac{2}{\sqrt{\pi}} \cdot \frac{H_0}{\cos\theta_i}$, this is 0.56 times the "usual" definition that assumes $2a = 2H_0$, and $2b = 2H_0/\cos\theta_i$.

4. DISCUSSION

Note that, despite Eqn. (9) has been often reported in the literature, its linkage to the bistatic radar equation is not that obvious, or at least this is what appears published. Equation (2b) also correctly describes the experimental evidence shown in Fig. 2, that the coherent reflected power is roughly independent of the platform height, since in the GNSS-R case the distance from the transmitter to the scattering area R_T is much larger than the distance from the scattering area to the receiverR_R . This means also that after a land scattering, the received power from a LEO will not differ much from that collected from s stratospheric balloon, around -158 dBm, that is, 25 dB less than the direct signal.

However, over the ocean, Martin et al. [11] using real experimental data from ground-based, airborne, and spaceborne scenarios, estimated that the ratio of the coherent to the incoherent components was ~3% for the ground-based experiment, ~0.4% for the airborne experiment, and just ~0.08% for the spaceborne one, which means that most likely this coherent component will only be detectable from space over land, ice, or almost calm ocean surfaces.

5. CONCLUSIONS

This work has proposed a unified GNSS-R scattering model that integrates the coherent (specular reflection) and incoherent (diffuse reflection) components of the scattered electromagnetic field over rough surfaces in a seamless way using the same analytic expressions of the power waveform (bistatic radar equation). The model explains the experimental data gathered in two stratospheric balloon experiments over boreal forests and lakes (BEXUS 17 and 19 on October 2013 and 2014) showing that: a) there is a detectable coherent component in the scattered signal whose amplitude is nearly constant with the receiver's height, and b) it has a multi-modal behaviour indicating that different scattering mechanisms are taking place. These findings in 2013 and 2014 triggered a change of paradigm in the field, that had neglected until then the existence of a coherent component, even at large incidence angles. This must be considered for present and future space-borne missions. In particular, the ^{3}Cat-2 6U CubeSat mission form the Universitat Politecnica de Catalunya aims at providing dual-band, dual-polarization multi-constellation data sets allowing the development of new algorithms to retrieve geophysical information measuring both the coherent scattered field and the incoherent component as well using different techniques. ^{3}Cat-2 will be launched at the end of July 2016.

6. REFERENCES

[1] S.T. Lowe, J.L. LaBreque, C. Zuffada, L.J. Romans, L.E. Young, and G.A. Hajj, "First Space-borne Observation of an Earth-Reflected GPS Signal", Radio Science, vol. 37, no. 1, pp. 7.1-7.28, 2002.

[2] S. Gleason, S. Hodgart, Y. Sun, C. Gommenginger, S. Mackin, M. Adjrad, and M. Unwin, "Detection and Processing of Bistatically Reflected GPS Signals from Low Earth Orbit for the Purpose of Ocean Remote Sensing", IEEE Transactions on Geoscience and Remote Sensing, vol. 43, no. 6, pp. 1229-1241, 2005.

[3] H. Carreno-Luengo, A. Amèzaga, A. Bolet, D. Vidal, J. Jané, J.F. Munoz, R. Olivé, and A. Camps, "Multi-Constellation, Dual-Polarization, and Dual-Frequency GNSS-R Stratospheric Balloon Experiment Over Boreal Forests", in Proceedings of the 2015 IEEE International Geoscience and Remote Sensing Symposium, pp. 5107-5110, Milan, Italy.

[4] V.U. Zavorotny, and A.G. Voronovich, "Scattering of GPS signals from the ocean with wind remote sensing application", IEEE Transactions on Geoscience and Remote Sensing, vol. 38, no. 2, pp. 951-964, 2000.

[5] C. Cox, and W. Munk, "Measurement of the Roughness of the Sea Surface from Photographs of the Sun's Glitter", J. Opt. Soc. Am., 14, 838–850, 1954.

[6] H. Carreno-Luengo, A. Camps, J. Querol and G. Forte, "First results of a GNSS-R experiment from a stratospheric balloon over boreal forests", IEEE Transactions on Geoscience and Remote Sensing, vol. 54, no. 5, pp. 2652 - 2663, 2015.

[7] H. Carreno-Luengo and A. Camps, "First dual-band multi-constellation GNSS-R scatterometry experiment over boreal forests from a stratospheric balloon", IEEE Journal of Selected Topics in Applied Earth Observations and Remote Sensing, vol.1, n.99, pp. 1-10, 2015.

[8] H. Carreno-Luengo, A. Amèzaga, D. Vidal, R. Olivé, J.F. Munoz, and A. Camps, "First polarimetric GNSS-R measurements from a stratospheric flight over boreal forests", MDPI Remote Sensing, vol. 7, no. 10, pp. 13120-13138, 2015.

[9] F.T. Ulaby, D.G. Long, *Microwave radar and radiometric remote sensing*. The University of Michigan Press, Ann Arbor, USA, 2014).

[10] J. A. Pogemiller, C.-C. Chun, D. Gebre- Egziabher, "A GPS bistatic radar for small satellite applications", in Procedeeings of the 23rd Annual AIAA/USU Conference on Small Satellites.

[11] F. Martin, A. Camps, F. Fabra, A. Rius, M. Martín-Neira, S. D'Addio, and A. Alonso, "Mitigation of Direct Signal Cross-Talk and Study of the Coherent Component in GNSS-R", IEEE Geoscience and Remote Sensing Letters, vol. 12, no. 2, pp. 279-283, 2015.

ACKNOWLEDGEMETNS: This project has received funding from the European Union's Seventh Framework Programme for research, technological development and demonstration under grant agreement "European GNSS-R Environmental Monitoring" no FP7-607126-E-GEM (Online Available: http://www.e-gem.eu), and by the project "AGORA: Técnicas Avanzadas en Teledetección Aplicada Usando Señales GNSS y Otras Señales de Oportunidad" of the Spanish Ministerio de Economía y Competitividad (MINECO/FEDER), Grant No ESP2015-70014-C2-1-R.